Scintillation Performance of Aliovalently-Doped $CeBr_3$

Mark J. Harrison, *Member, IEEE*, Christopher Linnick, Benjamin Montag, Samuel Brinton, Mark McCreary, F. P. Doty, and Douglas S. McGregor, *Member, IEEE*

***Abstract*—Strengthening the crystal lattice of lanthanide halides, which are brittle, anisotropic, ionic crystals, may prove to increase the availability and ruggedness of these scintillators for room-temperature gamma-ray spectroscopy applications. Eight aliovalent dopants for $CeBr_3$ were explored in an effort to find the optimal aliovalent strengthening agent. Eight dopants, $CaBr_2$, $SrBr_2$, $BaBr_2$, $ZrBr_4$, $HfBr_4$, $ZnBr_2$, $CdBr_2$, and $PbBr_2$, were explored at two levels of doping, 500 and 1000 ppm. From each ingot, samples were harvested for radioluminescence spectrum measurement and scintillation testing. Of the eight dopants explored, only $BaBr_2$ and $PbBr_2$ were found to clearly decrease total light yield. $ZnBr_2$ and $CdBr_2$ dopants both affected the radioluminescence emission spectrum very little as compared to undoped $CeBr_3$. $HfBr_4$- and $ZnBr_2$-doped $CeBr_3$ exhibited the highest light yields.**

***Index Terms*—Aliovalent doping, crystal growth, scintillation detectors, solid solution hardening.**

I. Introduction

CERIUM-ACTIVATED lanthanide halide scintillators, including but not limited to lanthanum chloride ($LaCl_3$), lanthanum bromide ($LaBr_3$), and cerium bromide ($CeBr_3$), are excellent candidates for applications in room-temperature gamma-ray spectroscopy. Total light yields are significantly greater than that for the industry-standard thallium-doped sodium iodide (NaI:Tl) and are typically reported to be in the range of 65,000–75,000 ph/MeV [1], [2]. These higher light yields coupled with better light yield proportionality than NaI:Tl give these scintillators superior energy resolution performance, which have been reported to be less than 3% FWHM at 662 keV [3] as opposed to the nominal 6–7% FWHM at 662 keV for NaI:Tl [4]. Additionally, the Ce radiative decay process ($\sim$ 30 ns) is far faster than the Tl decay ($\sim$ 250 ns) making these lanthanide halide scintillators attractive for timing applications as well.

Unfortunately, these lanthanide halides have several deleterious properties which limit their availability on the commercial market. Foremost is the fact that these materials possess a hexagonal crystal structure [5], which produces very anisotropic mechanical properties, such as thermal expansion [6]. Second, the ionic nature, low symmetry and weak bonding of these solids means they exhibit limited plasticity and brittle fracture, both of which play a key role in limiting the availability of the material by hindering crystal growth and increasing the difficulties associated with maintaining crystal integrity during remote use. Thus, this work was motivated by the need to improve the mechanical properties of $CeBr_3$ specifically and, in general, provide a path for strengthening scintillators without degrading scintillation performance.

While numerous methods are known for strengthening materials, only a few are applicable to ionic single crystals [7]. Solid solution hardening through aliovalent cation doping appears to be the most promising method since doping levels are typically quite low, 50–1000 ppm, to achieve considerable strengthening. The strain fields generated around an aliovalent impurity atom are tetragonal and considered to be "strong" barriers to dislocation motion. Further, the low levels of doping are less likely to interfere with the scintillation process. In other materials, aliovalent doping on the order of 100 –500 ppm, such as Y^{3+} in CaF_2, has been shown to increase the critical resolved shear stress (CRSS) by an order of magnitude [8].

The introduction of aliovalent impurities into a scintillating host can, however, have dire consequences for performance. Impurities may introduce energy states in the band gap of the host crystal which interfere with the charge carrier relaxation processes to quench light emission and/or decrease scintillation photon mean free path lengths through absorption or scattering. Thus, while strength may be dramatically improved, scintillation performance may also drastically degrade. Identifying those impurities which do not participate in nor deleteriously affect scintillation is the primary goal of this work.

In the following, the effects of eight different aliovalent cations on the scintillation properties of $CeBr_3$ are investigated. Ingots of $CeBr_3$ undoped and doped with each of the eight chosen dopants, $CaBr_2$, $SrBr_2$, $BaBr_2$, $ZrBr_4$, $HfBr_4$, $ZnBr_2$, $CdBr_2$ and $PbBr_2$, were grown via a horizontal gradient freeze method and compared to the undoped $CeBr_3$ through radioluminescence spectra and total light yields.

II. Theoretical Considerations

A. Dopant Selection

Despite the attractiveness of aliovalent doping to increase the CRSS of lanthanide halides, it is generally known that impurities exhibiting multiple stable valences quench the radiative Ce

Manuscript received November 13, 2008; revised January 22, 2009. Current version published June 17, 2009. This work was supported in part by the U.S. Department of Energy, Office of Nonproliferation Technology, Department NA22, Advanced Materials. Sandia is a multiprogram laboratory operated by Sandia Corporation, a Lockheed Martin Company, for the U.S. Department of Energy's National Nuclear Security Administration under Contract DE-AC04-94AL85000.

M. J. Harrison, C. Linnick, B. Montag, S. Brinton, M. McCreary, and D. S. McGregor are with the Semiconductor Materials and Radiological Technologies Laboratory, Kansas State University, Manhattan, KS 66506 USA (e-mail: harrison@ksu.edu; mcgregor@ksu.edu).

F. P. Doty is with Sandia National Laboratories, Livermore, CA 94551 USA (e-mail: fpdoty@sandia.gov).

Digital Object Identifier 10.1109/TNS.2009.2021057

relaxation mechanism, "killing" light production [9]. Thus, it is critical that only aliovalent ions exhibiting a single stable valence be chosen for scintillation purposes. As an exception to the above state rule, Pb^{2+} was included in the candidate list to affirm the quenching phenomenon. Pb is stable as both Pb^{2+} and Pb^{4+}, which was expected to "kill" the scintillation.

While many candidates exist, the scope of the investigation undertaken was limited to ions having stable valences of $2+$ or $4+$. This definition of scope therefore limited the investigation to Group II and Group IV elements. Another important consideration was cation size. Cations significantly smaller than Ce^{3+} will be less likely to incorporate themselves into the lattice and more likely to form secondary-phase precipitates due to solubility limitations. In 9-fold coordination, Ce^{3+} has an ionic radius of 1.196 Å [10]. Therefore, cations with only marginally different radii were investigated. However, size exceptions were made for Zr^{4+} and Hf^{4+} so that at least some tetravalent cations could be investigated.

Based on size and valence criteria, only five prime candidates met the stipulations, those being Ca^{2+}, Sr^{2+}, Ba^{2+}, Zn^{2+} and Cd^{2+}. Inclusion of the three exceptions, Zr^{4+}, Hf^{4+}, and Pb^{2+}, extended the candidate list to a total of eight dopants to investigate.

B. Effects On Scintillation

Assuming the dopant concentrations are below the solid solubility limits of $CeBr_3$, it is expected that the aliovalent dopants will incorporate themselves onto cation lattice sites and be closely associated with vacancies (divalent) or interstitials (tetravalent) [9]. However, since the doping levels are expected to far exceed the intrinsic concentrations of vacancies or interstitials in the host lattice, the vacancy or interstitial concentrations will necessarily be determined by doping levels. A substantial increase in point defects may act to capture charge carriers and thus alter the energy transfer mechanisms to the radiative centers.

While the close coupling between aliovalent impurities and their charge compensating defects is beneficial to material strengthening, the overall effect on scintillation may be deleterious. Ideally, the introduced dopants will not participate in nor affect the scintillation process. Nevertheless, it appears quite possible that many or all impurities will degrade scintillation efficiency.

III. Experimental Procedure

A. Crystal Growth

Several ingots, doped with either 500 ppm or 1000 ppm of each dopant, were first grown using a horizontal gradient freeze method in two 24-zone electro-dynamic gradient (EDG) furnaces. Quartz ampoules with an internal diameter of 25 mm were first loaded with 140 g of 99.999% pure, anhydrous $CeBr_3$ beads and the appropriate amount of anhydrous bromide dopant powder or beads of the highest purity available inside an ultra-dry atmosphere glove box purged with UHP N_2 gas. The ampoules were valve sealed and attached to a vacuum system for sealing. Ampoules were evacuated to 5×10^{-6} Torr or less and held at $100°C$ for at least 12 hrs, then flame sealed using an $H_2 - O_2$ torch.

Two sealed ampoules were then placed inside an EDG furnace with their plugged ends facing outward from the center of the furnace. The furnace was heated to $740°C$ and held for a minimum of 12 hrs to allow dopant mixing. Lastly, the outer zones were cooled in succession from $740°C$ to $700°C$ to obtain a growth rate of approximately 1.06 mm/hr.

B. Sample Preparation

Ingots were first carefully extracted from the quartz ampoules using a SiC disk saw to cut away the quartz and stored under mineral oil inside an ultra-dry atmosphere glove box. As-grown ingots were mounted to soft ceramic mounts for cutting using low melting point wax ($T_m = 60°C$). Samples were cut from the as-grown ingots with a diamond wire saw using mineral oil as the cooling fluid. During cutting, the hygroscopic ingots were constantly bathed in mineral oil to prevent degradation in open atmosphere.

Rough cut samples were then hand-lapped flat under mineral oil in open atmosphere using 1200 grit SiC lapping paper. Lapped samples were finally dried and hand-polished under an ultra-dry atmosphere using 4000 grit SiC paper. The completed samples appeared optically clear with smooth surfaces.

C. Radioluminescence Spectra Collection

Radioluminescence spectra for each dopant were collected by mounting a polished sample from each ingot inside a light-tight, N_2-purged project box. Light was collected and optically connected to an Ocean Optics USB4000 spectrophotometer calibrated with an LS-1 tungsten-halogen 3100 K light source. An x-ray generator was used to excite the samples. Before testing, a background spectrum was recorded then subtracted from the gross spectrum to obtain a net radioluminescence emission spectrum.

D. Total Light Yield Estimation

Total light yield was estimated for samples by comparing their ^{137}Cs spectra against a spectrum obtained with identical settings with a BGO crystal. To estimate the total light yield of the sample, two key corrections were taken into account. First, the light collection efficiency (ratio of the number of photons incident on the photocathode to the total number of photons emitted during the scintillation event) is related to several factors. Second, the spectral sensitivity of the photocathode must be taken into account to correct for changes in emission spectra between different scintillating materials.

To begin, the total charge collected at the anode of a PMT from light emitted by a scintillator can be estimated as

$$Q = E_\gamma Y \varepsilon I G, \tag{1}$$

where $E_\gamma(MeV)$ is energy deposited by a gamma-ray, Y is the total light yield of the scintillator in photons per MeV, ε is the light collection efficiency, I is the integral quantum efficiency of the photocathode to the spectral emission of the scintillator and G is the gain of the photomultiplier. If two samples, an unknown

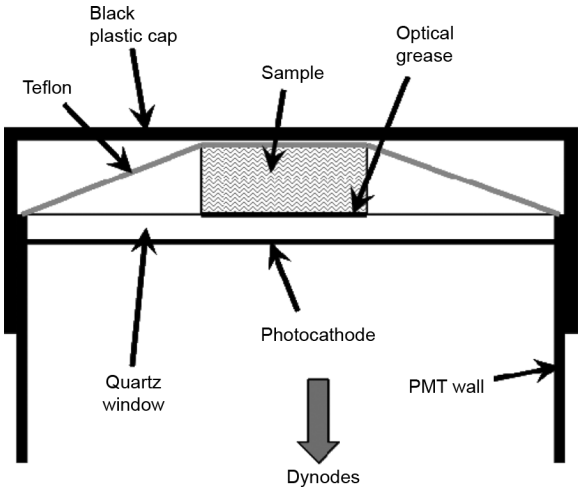

Fig. 1. Cross-sectional sketch of a sample scintillator crystal mounted to the Photonis XP5301 PMT as used to estimate total light yield.

and a known, are tested under identical gain settings, the ratio of their collected charges becomes

$$\frac{Q_x}{Q_s} = \frac{Y_x \varepsilon_x I_x}{Y_s \varepsilon_s I_s}, \tag{2}$$

where the subscripts x and s denote the unknown sample and the known standard respectively. Solving for the unknown sample's light yield, it is found

$$Y_x = Y_s \left(\frac{\varepsilon_s}{\varepsilon_x}\right)\left(\frac{I_s}{I_x}\right)\left(\frac{Q_x}{Q_s}\right). \tag{3}$$

Light collection efficiencies are difficult quantities to measure. However, Monte Carlo photon transport simulations can provide rough estimates. To estimate the light collection efficiencies of the samples studied here, the program DETECT2000 was used [11], [12]. Since surface characteristics of the samples were undetermined, DETECT2000 was used to provide only a relative measure between samples of differing size. Thus, while the absolute light detection efficiency of a given sample as simulated in DETECT2000 may be subject to question given the uncertainties in surface conditions, the relative change in light collection efficiency from one sample size to the next depends far less on surface finishes and reflector properties and more on the changes in geometry. Individual sample geometries and indices of refraction were used to estimate light collection efficiencies for each cuboid-shaped sample, including the known standard. The index of refraction for the doped $CeBr_3$ samples was assumed to be 1.95, similar to that for $LaBr_3:Ce$ [13].

The geometries simulated were cuboids of scintillator material of size matching the sample dimensions, a $50\,\mu m$ thick layer of optical grease, and a 1 mm thick layer of quartz to act as a PMT window. The top surface of the scintillator was specified as painted with a diffuse reflector (Teflon) with a reflection coefficient of 0.9. The outer, side surfaces of the scintillator material were specified as rough, while the coupled face was specified as optically smooth. Fig. 1 is a cross-sectional sketch of the experimental arrangement of the sample and Teflon on the PMT, which was approximated by the above described simulation parameters for estimating the light collection efficiency of each sample.

250,000 photons were generated uniformly throughout the scintillation sample volume with uniformly distributed initial directions. The number of photons incident upon the backside of the quartz window (photocathode) were counted. The ratio of emitted photons to incident photons was finally calculated and used as an estimate of light collection efficiency, ε.

The integral quantum efficiency is a ratio of the number of ejected photoelectrons from a photocathode to the number of incident photons with non-monochromatic distribution, $\Phi_{e,\lambda}$. Spectral quantum efficiency, ρ, is related to spectral sensitivity, $S_{k,\lambda}$, by

$$\rho = \left(\frac{hc}{e\lambda}\right) S_{k,\lambda}, \tag{4}$$

where h is Planck's constant, c is the speed of light in a vacuum, and e is the elementary charge [14]. From (4), I is determined by integrating and normalizing over all wavelengths in the manner

$$I = \frac{\int_0^\infty \rho \Phi_{e,\lambda} d\lambda}{\int_0^\infty \Phi_{e,\lambda} d\lambda}. \tag{5}$$

Here, $\Phi_{e,\lambda}$ is the radioluminescence intensity spectrum previously measured as described above.

Finally, samples were mounted to a Photonis XP5301 PMT with a small amount of optical grease, a layer of Teflon laid over the crystal (sides not covered) and sealed under a non-reflective, light-tight cap. The PMT output signal was first sent to an Ortec 113 preamplifier, then to a Canberra 2022 shaping amplifier. Amplifier output was finally directed into an Ortec Trump MCA. Each mounted sample was irradiated with ^{137}Cs and a scintillation spectrum recorded.

It was assumed that the peak height of the pulses input into the MCA was directly proportional to the quantity of charge collected at the PMT anode, i.e., $V \propto Q$. The centroid channel of the photopeak (Pk) in each spectrum was assumed to be linearly related to the input peak voltage with the form

$$Pk = mV + b. \tag{6}$$

Calibration of the MCA with a BNC pulser produced estimates of the MCA gain and offset of $m = 745.26\ chn/V$ and $b = -46.777\ chn$. Since V and Q are proportional,

$$\frac{V_x}{V_s} = \frac{Q_x}{Q_s}. \tag{7}$$

This relation in (7) implies that

$$Y_x = Y_s \left(\frac{\varepsilon_s}{\varepsilon_x}\right)\left(\frac{I_s}{I_x}\right)\left(\frac{V_x}{V_s}\right). \tag{8}$$

Utilizing (6) to predict input pulse heights from recorded channel numbers, (8) can be used to estimate total light yield of an unknown sample of size and shape differing from that of the standard known sample.

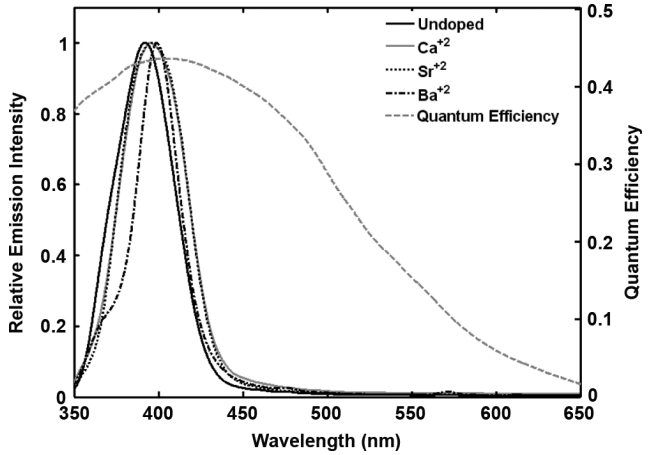

Fig. 2. Group IIA-doped $CeBr_3$ radioluminescence spectra.

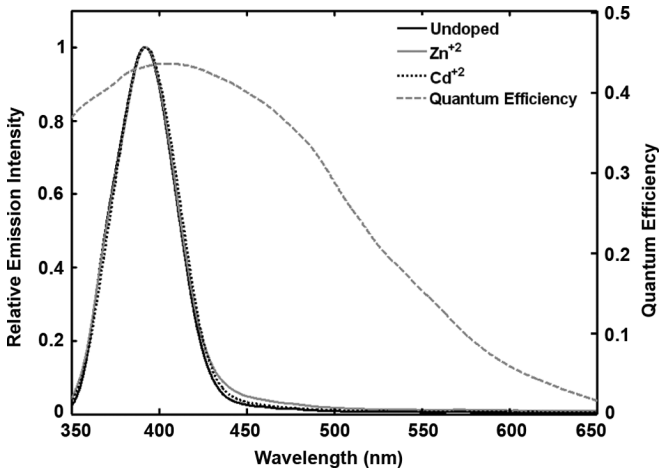

Fig. 3. Group IIB-doped $CeBr_3$ radioluminescence spectra.

IV. Results

A. Crystal Growth

Due to the relatively high thermal gradients in the gradient freeze method, the as-grown ingots contained a large number of visible internal arrested cracks running parallel to one another (presumably along the c-axis), indicating the strengthened alloys can support high grown-in stress. Furthermore, it was clearly observed that the single crystal yield from doped ingots was far greater than from undoped $CeBr_3$ ingots. Post-growth cracking was also observed to be dramatically reduced in the doped ingots, regardless of dopant.

B. Radioluminescence

The measured scintillation spectra for ingots doped with each aliovalent element are shown below in groups. Fig. 2 plots the emission spectra of the Group IIA-doped ingots alongside the spectral quantum efficiency of the XP5301 photocathode [15]. Here it is noted that Ca^{2+} and Sr^{2+} both shift the peak emission slightly toward longer wavelengths, while Ba^{2+} appears to have significantly altered the spectrum.

The Group IIB dopants, Zn^{2+} and Cd^{2+}, exhibited little to no effect on the emission spectra as shown in Fig. 3. However, Pb^{2+} drastically altered the emission spectrum as shown in Fig. 4. Finally, it is seen in Fig. 5 that the tetravalent cations, Zr^{4+} and Hf^{4+}, shifted the emission spectrum slightly to longer wavelengths as compared to undoped $CeBr_3$.

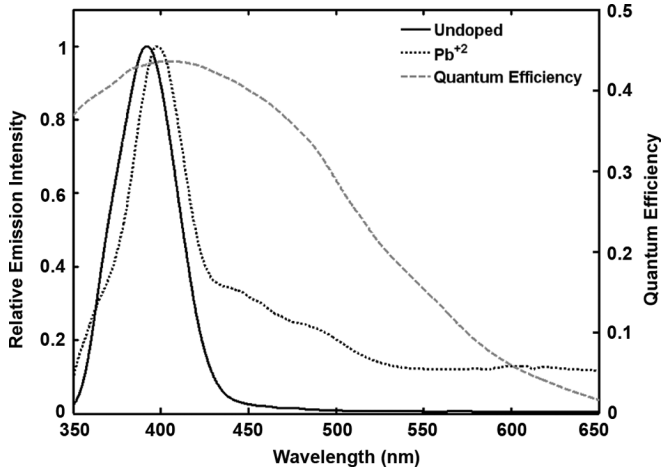

Fig. 4. Group IVA-doped $CeBr_3$ radioluminescence spectra.

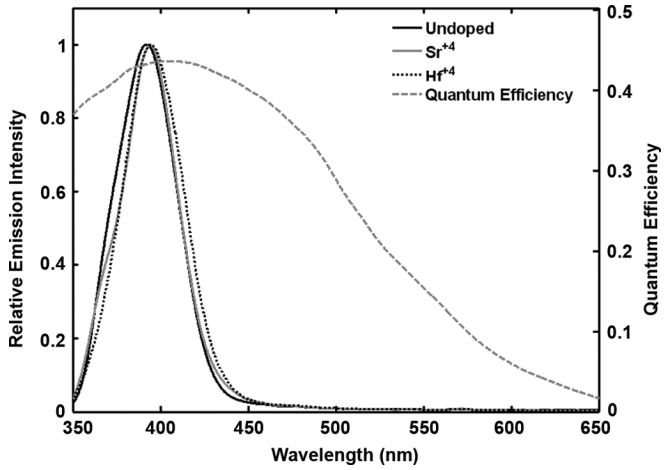

Fig. 5. Group IVB-doped $CeBr_3$ radioluminescence spectra.

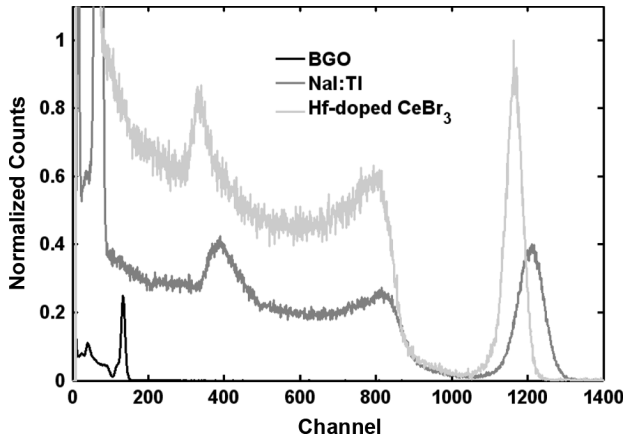

Fig. 6. Comparison of ^{137}Cs spectra collected using BGO, NaI:Tl and $LaBr_3:Ce$. Spectra have been normalized to their respective full energy peak and scaled to improve clarity.

C. Total Light Yields

The collected ^{137}Cs spectra for all samples were compared to BGO and, using (6) and (8), their total light yields were estimated at 662 keV. Fig. 6 is an example of the compared spectra, while Table I provides the final calculated maximum light yield

TABLE I
TOTAL LIGHT YIELD RESULTS

Material	Dopant	ε	I	Total LY
		(%)	(%)	(ph/MeV)
BGO	(Scionix)	52%	28.0%	6,850*
NaI(Tl)	(Harshaw)	49%	36.8%	50,000
$LaBr_3$	5% Ce	53%	36.8%	59,600
$CeBr_3$	1000ppm Ca	39%	39.8%	27,300
	500ppm Sr	47%	40.8%	43,300
	1000ppm Ba	41%	40.1%	35,100
	1000ppm Zr	47%	40.1%	46,300
	1000ppm Hf	41%	40.6%	52,500
	500ppm Zn	51%	39.1%	46,200
	1000ppm Zn	40%	39.1%	55,800
	500ppm Cd	53%	40.0%	44,500
	1000ppm Cd	40%	40.0%	38,500
	500ppm Pb	57%	30.7%	27,300

* BGO absolute light yield value assumed to be equal to that measured by Moszynski, et. al. [16] for a similarly sized sample.

TABLE II
SAMPLE DIMENSIONS

Material	Dopant	X	Y	Z
		(mm)	(mm)	(mm)
BGO	(Scionix)	10.6	10.1	3.9
NaI(Tl)	(Harshaw)	10.4	10.1	5.2
$LaBr_3$	5% Ce	10.8	7.6	2.9
$CeBr_3$	1000ppm Ca	5.2	5.0	4.3
	500ppm Sr	9.8	6.3	3.9
	1000ppm Ba	5.6	3.7	3.2
	1000ppm Zr	6.1	5.7	2.8
	1000ppm Hf	5.8	5.5	4.4
	500ppm Zn	7.0	6.0	2.1
	1000ppm Zn	8.0	6.0	5.9
	500ppm Cd	9.7	8.0	2.9
	1000ppm Cd	5.2	5.1	4.0
	500ppm Pb	11.9	10.7	2.8

values for each tested dopant and concentration. A commercial sample of NaI(Tl) was used as a measurement validation sample to confirm accuracy. The estimated light yield of the NaI(Tl) sample was 50,000 ph/MeV which matches reasonably well with that measured by de Haas and Dorenbos for a similarly sized and similarly mounted NaI:Tl crystal [1].

All samples were mounted on an XY-plane face as denoted in Table II.

V. CONCLUSIONS

The aliovalent dopants exhibited a wide range of effects on the radioluminescence emission spectrum. Pb^{2+} and Ba^{2+} exhibited the greatest effects on the radioluminescence spectrum. However, only Pb^{2+} altered the IQE with any significance, dropping it by nearly 10%. Zn^{2+} and Cd^{2+} had little to no effect on the emission spectrum. The remaining dopants were all observed to only slightly red shift the peak emission.

The measured light yields of all lanthanide bromide samples were lower than expected, despite the fact that the light yield measured for NaI(Tl) is reasonably accurate and falls within the margin of error of previous measurements [1]. Of the doped $CeBr_3$ samples, Hf^{4+} and Zn^{2+} appeared to yield the most light, although they were still 12% lower than that reported for undoped $CeBr_3$ [2]. Scattering losses due to microcracks caused by the high stress casting process are a possible cause to the reduced luminosity and is a subject for future investigation.

In-house grown, undoped $CeBr_3$, was not measured due to the lack of samples of sufficient quality. Unfortunately, the crystal growth method utilized did not produce single crystals of any useful size or clarity when the $CeBr_3$ was grown undoped. This fact implies two conclusions. First, the horizontal gradient freeze method of crystal growth is insufficient for producing high quality single crystals of undoped $CeBr_3$. Second, the dopants do appear to promote single crystal growth quite substantially.

While aliovalent doping does appear to be beneficial to improving ingot yields, work is underway to quantify the strengthening effect and will be reported when available.

ACKNOWLEDGMENT

The authors wish to thank Prof. Bill Dunn of the Radiation Measurement Applications Laboratory at Kansas State University for the use of their x-ray generator.

REFERENCES

[1] J. T. M. de Haas and P. Dorenbos, "Advances in yield calibration of scintillators," *IEEE Trans. Nucl. Sci.*, vol. 55, no. 3, pp. 1086–1092, Jun. 2008.

[2] K. S. Shah, J. Glodo, W. Higgins, E. V. D. van Loef, W. W. Moses, S. E. Derenzo, and M. J. Weber, "$CeBr_3$ scintillators for gamma-ray spectroscopy," *IEEE Trans. Nucl. Sci.* , vol. 52, no. 6, pp. 3157–3159, Dec. 2005.

[3] P. R. Menge, G. Gautier, A. Iltis, C. Rozsa, and V. Solovyev, "Performance of large lanthanum bromide scintillators," in *Nucl. Intrum. Methods Phys. Res. A*, 2007, vol. A579, pp. 6–10.

[4] G. Knoll, *Radiation Detection and Measurement*, 3 ed. New York: Wiley, 1999, p. 332.

[5] D. Brown, *Halides of the Transition Elements: Halides of the Lanthanides and Actinides*. New York: Wiley, 1968, p. 199.

[6] F. P. Doty, D. S. McGregor, M. J. Harrison, K. Findley, and R. Polichar, "Structure and properties of lanthanide halides," *Proc. SPIE*, vol. 6706, p. 670705, 2007.

[7] T. H. Courtney, *Mechanical Behavior of Materials*, 2 ed. Long Grove, IL: Waveland, 2000, ch. 5.

[8] M. N. Sinha and P. S. Nicholson, "Effect of impurities on the strengthening of CaF_2 single crystals," in *J. Mater. Sci.*, 1977, vol. 12, pp. 1451–1462.

[9] P. Lecoq, A. Annenkov, A. Gektin, M. Korzhik, and C. Pedrini, *Inorganic Scintillators for Detector Systems*. New York: Springer, 2006, pp. 88–89.

[10] G. S. Rohrer, *Structure and Bonding in Crystalline Materials*. Cambridge, U.K.: Cambridge Univ. Press, 2001, p. 521.

[11] F. Cayouette, D. Laurendeau, and C. Moisan, "DETECT2000: An improved Monte-Carlo simulator of the computer aided design of photon sensing devices," in *Proc. SPIE*, 2002, vol. 4833, pp. 69–76.

[12] F. Cayouette, N. Zhang, and C. J. Thompson, "Monte Carlo simulation using DETECT2000 of a multilayered scintillation block and fit to experimental data," *IEEE Trans. Nucl. Sci.*, vol. 50, no. 3, pp. 339–343, Jun. 2003.

[13] Saint Gobain Crystals BrilLanCe 380 Tech. Data Sheet, Saint Gobain Crystals, Hiram, OH, Jan. 2009 [Online]. Available: http://www.detectors.saint-gobain.com

[14] *Photomultiplier Tubes: Principles and Applications*, S. O. Flyckt and C. Marmonier, Eds. Brive, France: Photonis, 2002.

[15] Photonis Photomultiplier XP5301 Tech. Data Sheet, Photonis, Brive, France, Oct. 2007 [Online]. Available: http://www.photonis.com/upload/industryscience/pdf/pmt/XP5301.pdf

[16] M. Moszynski, M. Kapusta, M. Mayhugh, D. Wolski, and S. O. Flyckt, "Absolute light output of scintillators," *IEEE Trans. Nucl. Sci.*, vol. 44, no. 3, pp. 1052–1061, Jun. 1997.